

RESEARCH

Open Access



A novel cuproptosis-related gene model predicts outcomes and treatment responses in pancreatic adenocarcinoma

Qixian Liu, Ruiyu Li, Huanwen Wu* and Zhiyong Liang*

Abstract

Background Cuproptosis is recently emerging as a hot spot in cancer research. However, its role in pancreatic adenocarcinoma (PAAD) has not yet been clarified. This study aimed to explore the prognostic and therapeutic implications of cuproptosis-related genes in PAAD.

Methods Two hundred thirteen PAAD samples from the International Cancer Genome Consortium (ICGC) were split into training and validation sets in the ratio of 7:3. The Cox regression analyses generated a prognostic model using the ICGC cohort for training ($n = 152$) and validation ($n = 61$). The model was externally tested on the Gene Expression Omnibus (GEO) ($n = 80$) and The Cancer Genome Atlas (TCGA) datasets ($n = 176$). The clinical characteristics, molecular mechanisms, immune landscape, and treatment responses in model-defined subgroups were explored. The expression of an independent prognostic gene *TSC22D2* was confirmed by public databases, real-time quantitative PCR (RT-qPCR), western blot (WB), and immunohistochemistry (IHC).

Results A prognostic model was established based on three cuproptosis-related genes (*TSC22D2*, *C6orf136*, *PRKDC*). Patients were stratified into high- and low-risk groups using the risk score based on this model. PAAD patients in the high-risk group had a worse prognosis. The risk score was statistically significantly correlated with most clinicopathological characteristics. The risk score based on this model was an independent predictor of overall survival (OS) (HR = 10.7, $p < 0.001$), and was utilized to create a scoring nomogram with excellent prognostic value. High-risk patients had a higher *TP53* mutation rate and a superior response to multiple targeted therapies and chemotherapeutic drugs, but might obtain fewer benefits from immunotherapy. Moreover, elevated *TSC22D2* expression was discovered to be an independent prognostic predictor for OS ($p < 0.001$). Data from public databases and our own experiments showed that *TSC22D2* expression was significantly higher in pancreatic cancer tissues/cells compared to normal tissues/cells.

Conclusion This novel model based on cuproptosis-related genes provided a robust biomarker for predicting the prognosis and treatment responses of PAAD. The potential roles and underlying mechanisms of *TSC22D2* in PAAD need further explored.

Keywords Pancreatic adenocarcinoma, Cuproptosis, Risk model, Tumor microenvironment, Prognosis, Treatment response, Immunotherapy

*Correspondence:

Huanwen Wu
wuhuanwen10700@pumch.cn
Zhiyong Liang
liangzy@pumch.cn

Full list of author information is available at the end of the article



© The Author(s) 2023. **Open Access** This article is licensed under a Creative Commons Attribution 4.0 International License, which permits use, sharing, adaptation, distribution and reproduction in any medium or format, as long as you give appropriate credit to the original author(s) and the source, provide a link to the Creative Commons licence, and indicate if changes were made. The images or other third party material in this article are included in the article's Creative Commons licence, unless indicated otherwise in a credit line to the material. If material is not included in the article's Creative Commons licence and your intended use is not permitted by statutory regulation or exceeds the permitted use, you will need to obtain permission directly from the copyright holder. To view a copy of this licence, visit <http://creativecommons.org/licenses/by/4.0/>. The Creative Commons Public Domain Dedication waiver (<http://creativecommons.org/publicdomain/zero/1.0/>) applies to the data made available in this article, unless otherwise stated in a credit line to the data.

Introduction

Pancreatic adenocarcinoma (PAAD) has a 5-year survival rate of only approximately 10% [1, 2]. The poor prognosis is largely attributed to its high aggressiveness and resistance to existing therapies [3]. The conventional American Joint Committee on Cancer (AJCC) staging system is universally used to evaluate the patients' risk and treatment requirements [4]. Nevertheless, this classification is limited in that it primarily focuses on clinical and pathological features, without considering molecular factors. Despite great progress in developing therapies (including chemotherapy, radiation therapy, immunotherapy, and targeted therapy) for PAAD, only a small number of patients can benefit from these treatments [5, 6]. Unfortunately, validated biomarkers to identify subgroups that may benefit from these treatments have not yet been developed [7]. Therefore, more accurate and effective biomarkers are urgently needed for identifying "high-risk" patients and those who would benefit from different interventions, optimizing clinical outcomes of PAAD.

Copper is a vital nutrient involved in many biological processes. Recently, copper dyshomeostasis was found to play an important role in cancer [8]. On the one hand, copper accumulation has been reported to promote tumor proliferation, growth, angiogenesis, and metastasis [9, 10], including in pancreatic neuroendocrine tumors [11]. On the other hand, with the worldwide success of platinum (II) compounds in cancer chemotherapy, copper complexes might also serve as potential antitumor agents [10]. However, the underlying mechanism remains largely unknown. Recently, a new form of programmed cell death pathway was discovered, named cuproptosis. Excess copper induced cuproptosis, which was distinct from all other known cell death forms, such as apoptosis, necrosis, ferroptosis, and autophagy [12]. In cuproptosis, excess copper could directly bind to lipoylated protein in the tricarboxylic acid (TCA) cycle, leading to proteotoxic stress and cell death. Clinical trials have shown that cuproptosis induced by copper ionophores helped cancer patients with low lactate dehydrogenase (LDH) respond better to treatment [13]. Cuproptosis has shown its therapeutic implications due to the preferential selectivity in cancer cells compared to normal cells [12]. Of note, accumulating studies have reported that cuproptosis-related genes are closely implicated in tumorigenesis, progression, prognosis, and drug sensitivity [14–16]. However, the role of cuproptosis-related genes in PAAD remains unclear.

This study aimed to develop a prognostic and therapeutic indicator for PAAD. 35 cuproptosis-related genes were screened using the Cox regression analyses to construct a prognostic model for PAAD. The model's accuracy was also validated with three other cohorts. We

then investigated the correlations between the risk score based on the model and clinicopathological characteristics, and explored the independent prognostic role of the risk score in PAAD. A comprehensive comparative analysis of the molecular and immune landscapes, as well as the response of immunotherapy, targeted therapy, and chemotherapy between different risk groups, was also carried out. Besides, an independent prognostic predictor *TSC22D2* in PAAD was identified from the model, and its expression was verified by public databases and experiments. Our study provided an effective prognostic model based on cuproptosis-related genes and facilitated personalized therapy for PAAD patients.

Materials and methods

Data source

In total, transcriptomic information and clinical data of 472 PAAD patients are derived from three independent public datasets, including 213 samples in the International Cancer Genome Consortium (ICGC)-PACA-CA (<https://dcc.icgc.org/releases/current/Projects>), 79 samples (GSE85916) in Gene Expression Omnibus (GEO) (<https://www.ncbi.nlm.nih.gov/geo/>), and 176 samples in The Cancer Genome Atlas (TCGA)-PAAD cohort. The latest gene expression profiles and corresponding clinical follow-up information from the TCGA were downloaded through the UCSC Xena genome browser database (<https://xenabrowser.net/datapages/>) [17]. The download time of these datasets was April 14, 2022. Below were the steps involved in processing these data: 1) Samples without survival status, survival time, and clinical follow-up information was picked out from the analyses. 2) Genes with multiple gene symbols were averaged using the median expression. 3) Genes with Ensembl IDs were converted to gene symbols. 4) The gene expression data were transformed to the $\log_2(\text{TPM} + 1)$ format.

213 samples of the ICGC-PACA-CA dataset were randomly divided into a training set ($n = 152$, 70%) and a validation set ($n = 61$, 30%). In case of the random division bias, the `createDataPartition` function of the "caret" R package was adopted to pre-randomize 213 samples 1000 times in advance. The division of the training set and validation set was unbiased because there is no difference in several features between the two sets, such as overall survival (OS), gender, age, AJCC stage, and histological grade (Supplementary Table 1). Besides, the testing set included samples from the TCGA-PAAD cohort and the GSE85916 cohort.

Construction and validation of a prognostic model related to cuproptosis

A list of previously reported 35 cuproptosis-related genes was shown in Supplementary file 1 [12]. 34

cuproptosis-related genes were successfully matched with the training set. Univariate Cox regression analysis was used in the training set to explore the prognostic relevance of these genes for OS through the `coxph` function of the “survival” R package [18]. Then, a multivariate Cox regression analysis was conducted to obtain the coefficient of each gene for establishing the formula of the risk score. Patients were divided into two risk groups based on the median value of the risk score. Finally, the “timeROC” package was used in three additional datasets to analyze the specificity and sensitivity of 1-, 2-, and 3-year OS predictions. The area under the curve (AUC) was calculated to assess the ROC effect. The Kaplan–Meier (KM) curve analysis [19] was established by the “survminer” package to compare the OS between the high- and low-risk groups in the training, validation, and testing sets.

Clinical correlation and prognostic values of the model

The correlations between the risk score and clinical characteristics were visualized by violin plot using the “ggplot2” package. Univariate and multivariate Cox regression analyses were used to evaluate the independent prognostic value of the 3-gene signature model and other clinical characteristics (tumor grade, T stage, N stage, gender, age, and AJCC stage). The results of univariate and multivariate Cox analyses based on the TCGA

cohort were displayed as a forest plot by the “forestplot” package.

Construction and validation of the nomogram model

The “rms” package was used to create a nomogram based on the independent prognostic factors in the multivariate Cox regression analysis [20]. Every variable in the nomogram scoring system was given a score, and the total score was calculated by adding all the scores together. A calibration curve was drawn to show the consistency of the nomogram prediction and clinical observation in one-, two-, and three-year OS.

Analyses of the molecular and immune characteristics

“DESeq2” package was used to identify the differentially expressed genes (DEGs) between the high- and low-risk groups in the TCGA dataset. $|\text{Log}_2\text{FoldChange}| > 1$ and a false discovery rate (FDR)-adjusted P -value < 0.01 were set as the cutoffs for the DEGs. Results were visualized in a volcano plot using the “ggplot2” package. Gene ontology (GO) functional enrichment analyses were performed on these DEGs with the “clusterProfiler” package [21]. Data on genetic alternations were downloaded from the TCGA data portal (<https://portal.gdc.cancer.gov>). The MutSig2.0 approach [22] was used to identify significantly mutated genes, and the top mutated genes in two risk groups were visualized by the “Maftools” package

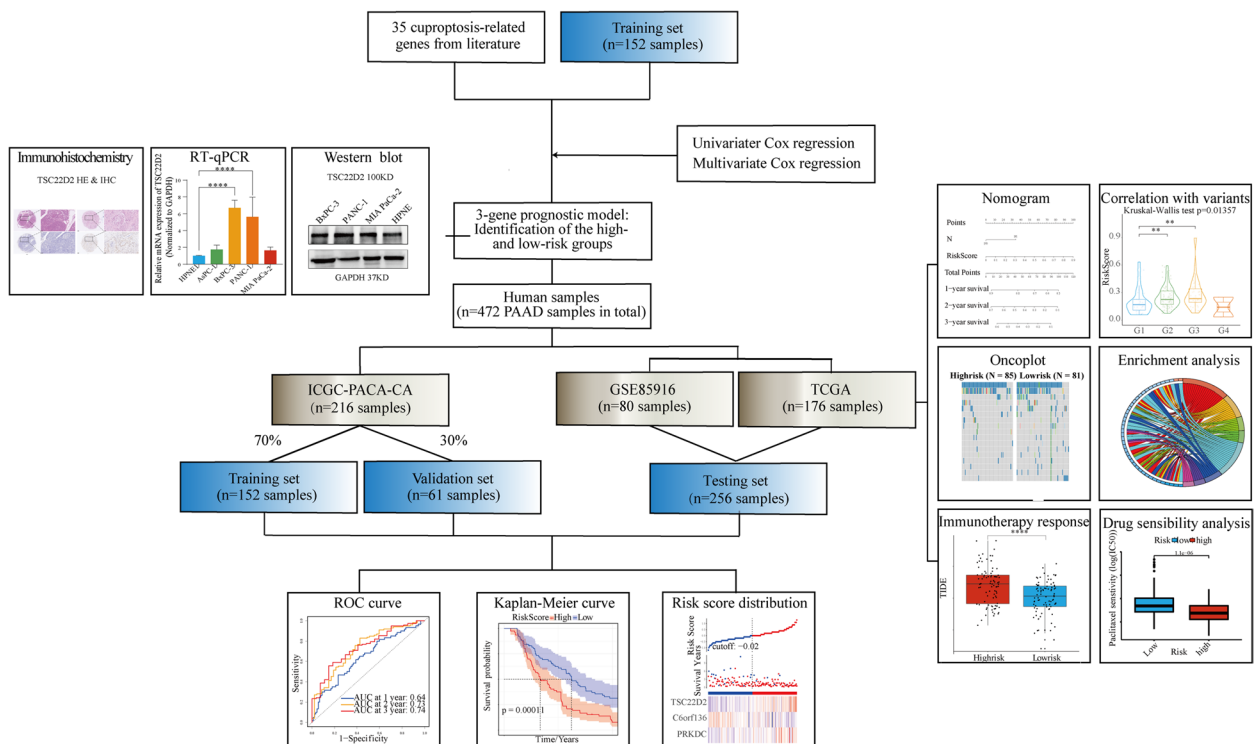


Fig. 1 The overall study design and workflow

[23]. Correlation analysis was constructed between the risk score and total mutation burden (TMB). The differences in TMB and microsatellite instability (MSI) score between the two risk groups were also visualized by boxplot using the “ggplot2” package. Moreover, twenty-two subpopulations of tumor-infiltrating immune cells were analyzed using the CIBERSORT algorithm (<https://cibersort.stanford.edu/>) [24]. The different expressions of some immune checkpoints in the high- and low-risk groups were detected, such as CD274, CD276, CD44, and CD40.

Prediction of treatment responses

In the immunotherapy response analyses, immunophenoscore (IPS) was a superior predictor of response to anti-cytotoxic T lymphocyte antigen-4 (CTLA-4) and anti-programmed cell death protein 1 (PD-1) antibodies [25]. IPS, available through The Cancer Immunome Atlas (TCIA) (<https://tcia.at/>), is developed from four categories: effector cells (activated CD4+ T cells, activated CD8+ T cells, effector memory CD4+ T cells, and effector memory CD8+ T cells), suppressive cells (Tregs and MDSCs), MHC-related molecules, and checkpoints or immunomodulators. Tumor Immune Dysfunction and Exclusion (TIDE) was calculated online (<http://tide.dfci.harvard.edu/>) and had potential clinical efficacy to assess the responsiveness of patients in different risk groups to immune checkpoint inhibitors (ICIs) therapy. The TIDE score is superior to recognized immunotherapy biomarkers (PD-L1 level, and interferon γ) for assessing anti-PD1 and anti-CTLA4 effectiveness. The responses to chemotherapy and target therapy were assessed using the “pRRophetic” package based on the Genomics of Drug Sensitivity in Cancer (GDSC) website (<https://www.cancerrxgene.org/>). A lower half-maximal inhibitory concentration (IC50) referred to a higher sensitivity to the drug treatment.

Exploration of the expression and prognostic value of TSC22D2 in public datasets

GEPIA (<http://gepia.cancer-pku.cn/>) was used to investigate the mRNA expression of hub genes involved in the prognostic model in tumor samples ($n = 179$) and normal samples ($n = 171$). Patients were divided into two groups based on the median expression of the hub gene. The

prognostic capabilities of these hub genes were respectively demonstrated using the KM curve in the TCGA, and ICGC datasets. To evaluate the expression of the hub gene at the protein level, we obtained the TCGA-PAAD proteomics cohort from the Clinical Proteomic Tumor Analysis Consortium (CPTAC), (<https://proteomics-cancer.gov/programs/cptac>) including tumor samples ($n = 137$) and normal samples ($n = 74$).

Validation of TSC22D2 RNA and protein expression in cell lines

Pancreatic cancer cell lines (AsPC-1 and BxPC-3) were cultured in RPMI-1640 (Corning, NY, USA) with 10% fetal bovine serum (FBS) and 1% penicillin–streptomycin. Two additional pancreatic cancer cell lines (PANC-1, MIA Paca-2) were cultured in DMEM (Dulbecco’ modified eagle medium) (Gibco, Grand Island, NY, USA) supplemented with 10% FBS and 1% penicillin–streptomycin. Human pancreatic ductal epithelium (hTERT-HPNE) cells were cultured in Medium D with mixtures of M3 and DMEM medium containing one volume of medium M3TM Base F culture media (InCell Corp., San Antonio, TX, USA), three volumes of glucose-free DMEM, 5% FBS, 5.5 mM glucose, 10 ng/ml EGF, and 50 μ g/ml gentamycin [26]. All these cells were cultured at 37 °C in a humidified atmosphere containing 5% CO₂. RNA was extracted from tissues using the TRIzol reagent (Invitrogen, Carlsbad, CA, USA) and was reverse-transcribed into cDNA using the PrimeScript RT Master Mix (Takara, Otsu, Shiga, Japan). RT-qPCR analyses were quantified with PowerUp™ SYBR® Green Master Mix (Applied Biosystems, Austin, TX, USA), and expression levels were normalized to *GAPDH* levels. Proteins were extracted in RIPA buffer supplemented with a complete, EDTA-free protease and phosphatase inhibitor single-use cocktail (Thermo Scientific). Proteins were separated by SDS-PAGE and blotted onto a PVDF membrane. Anti-TSC22D2 (1:1000 dilution, #25,418–1-AP, Proteintech) was used as primary antibodies for immunoblotting. Reacted antibodies were detected using an enhanced chemiluminescence detection system.

Statistical analysis

Categorical variables were analyzed using Fisher’s exact test or chi-square test. Continuous variables were analyzed by Wilcoxon rank-sum test or Kruskal–Wallis H

(See figure on next page.)

Fig. 2 Construction and validation of the prognostic model in the training and validation sets. **A** The risk score, survival time, survival status, and 3-gene expression trend in the training set (ICGC, 152 samples). **B** ROC curves for the sensitivity and specificity of one-, two-, and three-year OS according to the risk score in the training set. **C** Kaplan–Meier curve for OS between the high- and low-risk groups in the training set. **D** The risk score, survival time, survival status, and 3-gene expression trend in the validation set (ICGC, 61 samples). **E** ROC curves for the sensitivity and specificity of one-, two-, and three-year OS according to the risk score in the validation set. **F** Kaplan–Meier curve for OS between the high- and low-risk groups in the validation set

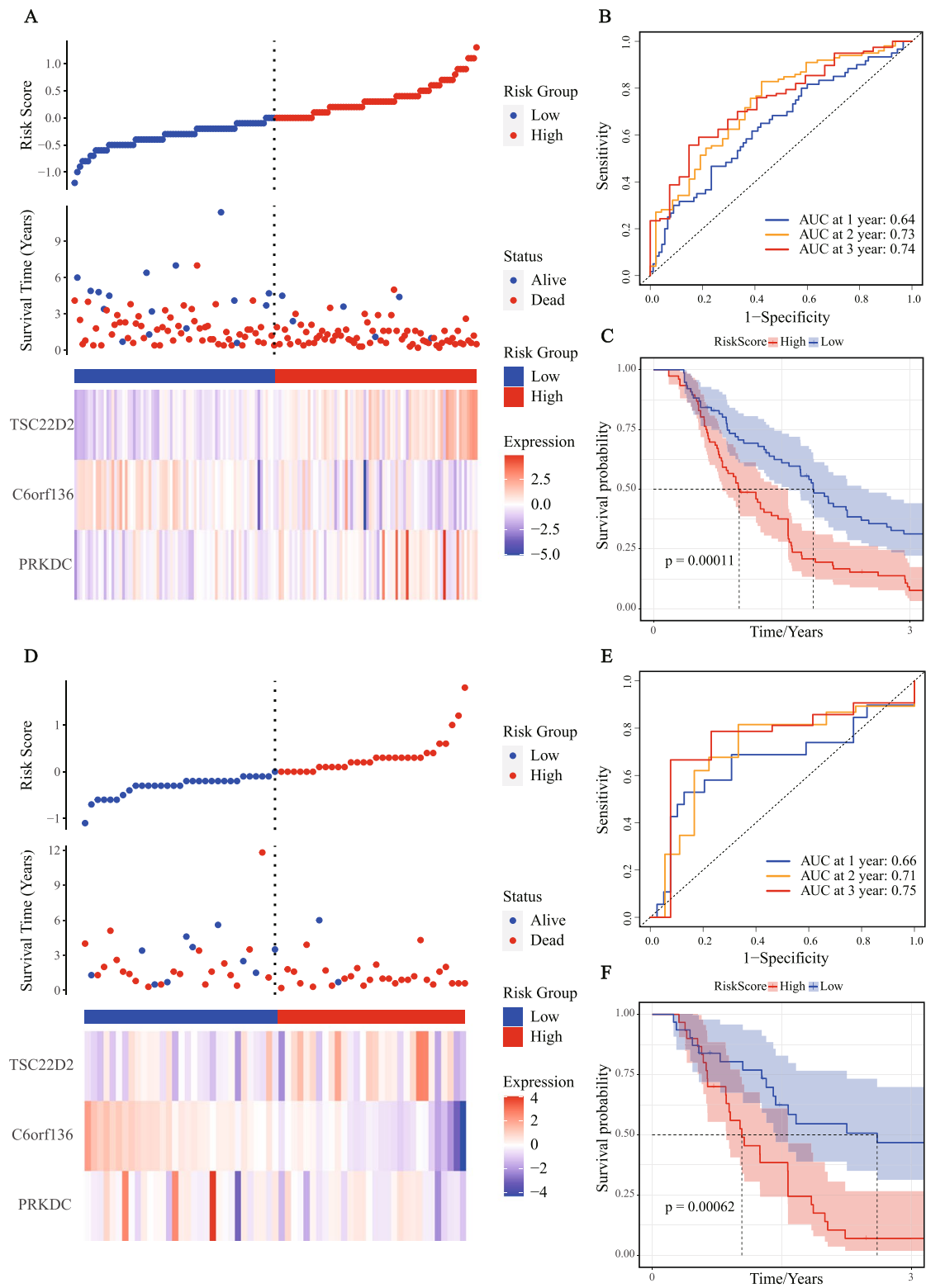


Fig. 2 (See legend on previous page.)

test. Correlations between two continuous variables were examined by Spearman's correlation analysis. All the statistical analyses were conducted by R software (version 4.1.3) and GraphPad Prism 8.0 (GraphPad Software Inc., San Diego, CA, The United States). All statistical tests were two-tailed unless otherwise stated. $P < 0.05$ were regarded as statistically significant.

Results

Constructing a prognostic model based on cuproptosis-related genes in the training set

An overview of the main design of the present study was shown in Fig. 1. Among 34 cuproptosis-related genes, only three genes (*TSC22D2*, *C6orf136*, and *PRKDC*) were significantly associated with the OS of PAAD patients in the univariate Cox regression. The results of multivariate Cox regression were shown in Supplementary Fig. 1. It revealed that *PRKDC* (hazards ratios [HR] 1.34, 95%CI 1.10–1.63, $p = 0.003$), *C6orf136* (HR 0.71, 95%CI 0.54–0.92, $p = 0.011$), *TSC22D2* (HR 1.85, 95%CI 1.35–2.53, $p < 0.001$) contributed significantly to OS. Both *PRKDC* and *TSC22D2* were risk factors with $HR > 1$, whereas *C6orf136* was a protective factor with $HR < 1$. Then, a prognostic model was constructed for all samples using the formula based on the risk coefficients of these three genes:

$$\text{Risk score} = 0.035 \times e^{(0.292 \times PRKDC - 0.347 \times C6orf136 + 0.613 \times TSC22D2)}$$

Taking the median risk score as the cut-off value, 152 samples in the ICGC-training set were divided into the high-risk group ($n = 76$) and the low-risk group ($n = 76$). The distribution of the risk score showed that more death events were observed in the high-risk group (Fig. 2A). As the risk score increased, the expression of *TSC22D2* and *PRKDC* also elevated obviously, while the expression of *C6orf136* had a notable downward trend. Based on the ROC analysis, our model had a great prediction performance for OS in the training set (AUC of 1-year OS = 0.64; AUC of 2-year OS = 0.73; AUC of 3-year OS = 0.74, Fig. 2B). KM curve analysis in the training set revealed that patients in the high-risk group had a worse prognosis than those in the low-risk group ($p = 0.00011$, Fig. 2C).

(See figure on next page.)

Fig. 3 Evaluation of prognostic model in the TCGA-testing set and functional enrichment analysis of DEGs between the risk groups. **A** The risk score, survival time, survival status, and 3-gene expression trend in the testing set (TCGA, 176 samples). **B** ROC curves for the sensitivity and specificity of one-, two-, and three-year OS according to the risk score in the testing set. **C** Kaplan–Meier curve for OS between the high- and low-risk groups in the testing set. **D** Volcano plot of DEGs between the high-risk and low-risk groups from TCGA data set. **E** The Chord of eight significantly enriched GO terms between high-risk and low-risk groups

Evaluating the prognostic model in the validation set and testing set

All 61 samples in the ICGC-validation set were divided into the high-risk ($n = 30$) and the low-risk ($n = 31$) groups based on the median risk score using the risk formula. The risk score distribution was plotted in the validation set, which indicated that a higher risk score was associated with more death events (Fig. 2D). Subsequently, ROC curves were plotted, and the 1-year, 2-year, and 3-year AUCs of the OS prediction in the validation set were 0.66, 0.71, and 0.75, respectively (Fig. 2E). Then, KM curve analysis showed patients with a higher risk score tended to have a significantly worse prognosis than the low-risk group ($p = 0.00062$, Fig. 2F).

To further verify the robustness of our 3-gene prognostic model, 176 samples from the TCGA-PAAD dataset and 79 samples from the GSE85916 dataset were used as the testing set. The above analyses were also conducted separately in these two datasets. The distribution of the risk score also showed that the high-risk group tended to have a higher risk of death. The expression trends of three genes in the testing set (TCGA-PAAD cohort, Fig. 3A; GSE85916 cohort, Supplementary Fig. 2A) were consistent with that in the training and validation set. The 1-year, 2-year, and 3-year AUCs of this model in the TCGA-testing set were 0.61, 0.64, and 0.71, respectively

(Fig. 3B). Besides, the 1-year, 2-year, and 3-year AUCs of the OS prediction in the GSE85916 testing set were 0.53, 0.62, and 0.68, respectively (Supplementary Fig. 2B). KM curve analysis revealed that the clinical outcomes of patients in the high-risk group were significantly worse ($p = 0.024$ in the TCGA-PAAD dataset, Fig. 3C; $p = 0.05$ in the GSE85916 dataset, Supplementary Fig. 2C).

To investigate the underlying mechanisms of the prognostic model, we performed a GO enrichment analysis of DEGs in the TCGA cohort. A total of 342 upregulated genes and 1149 downregulated genes were identified in the high-risk group ($|\log_2\text{FoldChange}| > 1$, $p < 0.01$), as shown in the volcano plot (Fig. 3D). A chord was plotted to show the functional enriched GO terms with $p\text{-value} < 0.01$ & $\text{FDR} < 0.01$ as the threshold (Fig. 3E).

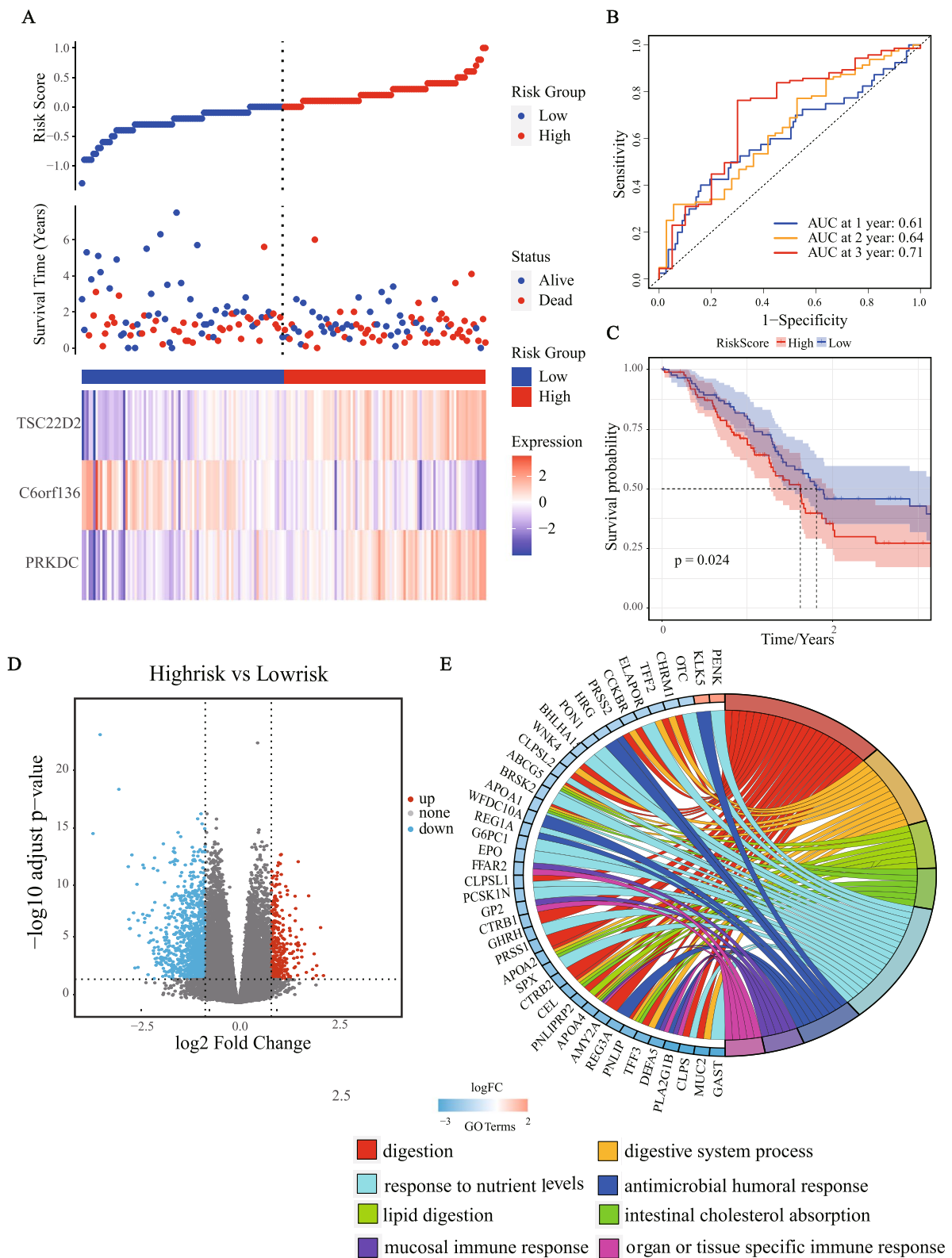


Fig. 3 (See legend on previous page.)

Interestingly, some immune response-related pathways were significantly enriched.

Exploring the correlation between the risk score and clinicopathological features

The risk score was calculated in the TCGA cohort to examine its correlation with clinicopathological features (Fig. 4A-F). The risk score was significantly related to tumor grade, AJCC stage, T stage, and N stage ($p < 0.05$). Patients with higher risk score tended to have a higher tumor grade and AJCC stage, a higher risk of lymphatic metastasis, and a larger tumor size. Patients under 65 years also had an increased risk score ($p < 0.05$). It is consistent with the previous cognition that younger PAAD patients may have a higher degree of tumor malignancy and a worse prognosis. Thus, our prognostic model provided a reliable prediction of clinicopathological characteristics.

Assessing the independent prognostic value and prognostic accuracy of the model

To investigate whether the risk score based on the prognostic model was an independent prognostic factor, we performed univariate and multivariate Cox regression analyses in the TCGA-PAAD set. Univariate Cox regression analysis showed that T stage, N stage, and the risk score based on the prognostic model were significantly associated with OS ($p < 0.05$, Fig. 4G). Meanwhile, multivariate Cox regression analysis revealed that the risk score based on the prognostic model was the only independent prognostic indicator of OS (HR=10.7, $p < 0.001$, Fig. 4H), which verified the robustness of our prognostic model again.

To make the prognostic model more clinically applicable, we constructed a nomogram model (Fig. 4I). The nomogram model was established using the N stage and the risk score since the risk score was highly significant ($p < 0.001$) and the N stage was marginally significant ($p = 0.055$) upon the multivariate Cox analysis. Both two elements were used to calculate each patient's total score, predicting PAAD patients' 1-year, 2-year, and 3-year survival probabilities. A calibration curve was plotted to analyze the consistency between the actual measured prognostic value and the prediction value by the nomogram. As shown in Fig. 4J, calibration curves of 1-year, 2-year, and 3-year OS in the TCGA cohort were near-optimal performance, which

indicated that the prediction performance of the nomogram was great.

Comparing the molecular characteristics and immune landscapes between the high- and low-risk groups

The mutation profiles were analyzed and compared between the high- and low-risk groups. The top17 mutations in known driver genes of PAAD were displayed in the oncoplot (Fig. 5A). Missense mutations were the most common mutation type, followed by frameshift deletions and nonsense mutations. The mutation rates of the top four mutated genes (*KRAS*, *TP53*, *SMAD4*, and *CDKN2A*) were all higher than 15% in both groups. The mutation rate of the TP53 gene was significantly more common in the high-risk group ($p < 0.01$), while the mutation rate of *TTN*, *RYR1*, and *GNAS* genes was more common in the low-risk group ($p < 0.05$).

Subsequently, we explored the correlation of the risk score with TMB and MSI. As a result, the risk score was negatively correlated with TMB ($R = -0.166$, $p < 0.05$, Supplementary Fig. 3A). The high-risk group had a significantly lower TMB score ($p < 0.05$, Fig. 5B), while there was no significant difference in MSI score between the two risk groups (Supplementary Fig. 3B).

As immune response-related pathways are associated with risk groups based on the model, we analyzed the distribution of 22 immune cells to compare the tumor microenvironment (TME) between two risk groups (Fig. 5C). Eosinophils and activated Natural killer (NK) cells were more abundant in the low-risk group, while activated dendritic cells and activated memory CD4 T cells were more plentiful in the high-risk group. Given the importance of ICIs in treating PAAD, we collected immunomodulatory genes for PAAD from previous literature and analyzed their expression in the two risk groups respectively (Supplementary Fig. 3C). As a result, almost all the immune checkpoint molecules were significantly higher in the high-risk group than in the low-risk group ($p < 0.05$).

Predicting treatment responses based on risk groups

IPS was utilized to analyze the relationship between the risk groups and immune response. In the TCGA cohort, the low-risk group had a significantly higher IPS than that in the high-risk group ($p < 0.001$, Fig. 5D), indicating patients in the low-risk group may have a better response

(See figure on next page.)

Fig. 4 The clinical implications and prognostic role of the model. **A-F** Correlation between the risk score and various clinical characteristics. **G** Univariate Cox analysis of the risk score and clinical characteristics for OS in the TCGA cohort. **H** Multivariate Cox analysis of the risk score and clinical characteristics for OS in the TCGA cohort. **I** The nomogram built in combination with the risk score and the N stage predicted one-, two-, and three-year OS in the TCGA cohort. **J** The probabilities of OS at one-, two-, and three-year were assessed by the calibration curve of the nomogram in the TCGA cohort. * $p < 0.05$; ** $p < 0.01$; *** $p < 0.001$; **** $p < 0.0001$

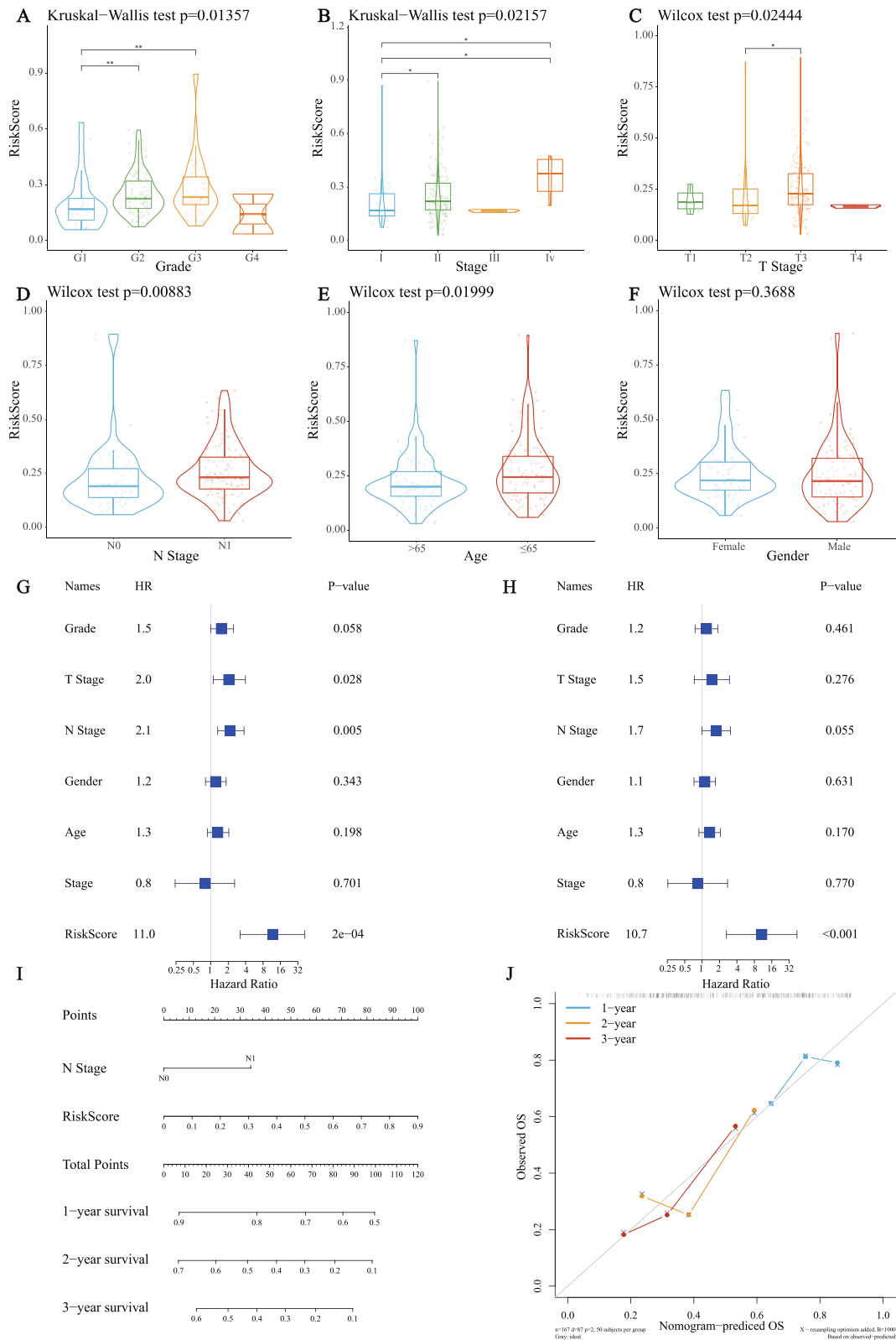


Fig. 4 (See legend on previous page.)

to ICIs. Besides, TIDE was also used to assess the potential clinical efficacy of immunotherapy in different risk groups. A higher TIDE score indicated a higher probability of tumor immune escape and thus inferior benefits from ICIs. Moreover, a higher TIDE score was related to a worse outcome. As shown in Fig. 5E, the high-risk group had a significantly higher TIDE prediction score than the low-risk group ($p < 0.0001$).

Chemotherapy and targeted therapy are important parts of multimodality treatment for pancreatic cancer [27]. However, due to the high resistance to chemotherapy and targeted therapy, many patients might not benefit from these treatments [28]. Thus, a total of 251 drugs from the GDSC website were estimated for chemotherapy and targeted therapy sensitivity in the high-risk and low-risk groups in the TCGA cohort. As shown in Fig. 6A-I, nine drugs had significantly different sensitivity between the two risk groups, including four chemotherapeutic agents (Paclitaxel, Zibotentan, Vinorelbine, Bexarotene), four targeted cancer drugs (Midostaurin, Pazopanib, Sorafenib, Imatinib), and a proteasome inhibitor (Bortezomib). The IC50 values of these chemotherapeutic agents and targeted therapies were significantly lower in the high-risk group ($p < 0.001$), indicating that patients in the high-risk group were more sensitive to these drugs.

Identifying high expression of *TSC22D2* as a novel prognostic indicator in PAAD

We screened each gene of our 3-gene prognostic model through KM curve analysis, respectively. Only *TSC22D2* was discovered to be significantly related to the prognosis of PAAD both in the ICGC and TCGA cohorts. High expression of *TSC22D2* was significantly associated with a worse prognosis in ICGC-PACA-CA samples ($p < 0.001$, Fig. 7A), which was similar in the TCGA-PAAD samples ($p < 0.05$, Supplementary Fig. 4A).

Next, data from CPTAC was obtained to investigate the expression of *TSC22D2* at the protein level. The protein expression of *TSC22D2* was significantly higher in PAAD samples ($n = 137$) than that in normal samples ($n = 74$) ($p < 0.001$), as shown in Fig. 7B. In addition, we analyzed the expression of *TSC22D2* at the RNA level. As shown in Fig. 7C, data from GEPIA showed that *TSC22D2* gene expression was significantly upregulated in pancreatic cancer tissues ($n = 179$) than that in normal tissues ($n = 171$) ($p < 0.001$).

Our western blot results revealed that pancreatic cancer cell lines (BxPC-3, PANC-1, MIA PaCa-2) had higher *TSC22D2* protein expression than hTERT-HPNE (Fig. 7D). *TSC22D2* protein level was 48.8% ($p < 0.01$) higher in MIA PaCa-2 and 28.8% ($p < 0.001$) in PANC-1 than in control group (HPNE). The differential mRNA expression was also verified by RT-qPCR assays (Fig. 7E). The mRNA levels of *TSC22D2* were increased among all four pancreatic cancer cells as compared to HPNE control. Besides, BxPC-3 and PANC-1 have significantly higher expression levels than HPNE ($p < 0.0001$). The differential expression was consistent with the results from the Cancer Cell Line Encyclopedia (CCLE) database (Supplementary Fig. 4B). In addition, we detected the expression of *TSC22D2* in pancreatic cancer tissues and paired paratumor normal tissues by immunohistochemistry (IHC) staining (Fig. 7F). The results showed that *TSC22D2* was significantly up-regulated in pancreatic cancer tissues compared with controls. Further explorations of its potential mechanism are currently investigating by us. Thus, an independent prognostic predictor of PAAD is *TSC22D2* high expression, and *TSC22D2* expression was also higher in pancreatic cancer tissues/cells than in normal tissues/cells.

Discussion

PAAD is a highly malignant cancer with a very dismal prognosis [29]. The development of immunotherapy, targeted therapy, and chemotherapy for PAAD has been boosted, as molecular biology and immunology advanced [30–32]. A personalized treatment was urgently needed to maximize the effectiveness of diverse treatment options [33]. After decades of research on biomarkers for PAAD, reliable biomarkers for identifying “high-risk” PAAD patients and those who would benefit from treatments are still lacking [34, 35]. As a new type of cell death, cuproptosis may provide new insights for biomarker development of PAAD [12, 13, 16]. In our study, the Cox regression analyses were applied to establish a 3-gene prognostic model, which was an independent prognostic factor for OS. We then explored the clinical implications of the prognostic model and analyzed its predictive ability for various treatment responses, including immunotherapy, chemotherapy, and target therapy. In addition, high expression of *TSC22D2* was discovered

(See figure on next page.)

Fig. 5 Comparing the molecular characteristics and immune landscapes between the high- and low-risk groups. **A** The oncoplot of somatic mutations in high- and low-risk patients using the TCGA cohort. **B** TMB between the high- and low-risk patients from the TCGA cohort. **C** Estimation of the proportions of immune infiltration cells using the CIBERSORT algorithm between the high- and low-risk groups. **D** The IPS score between the high- and low-risk patients from the TCGA cohort. **E** The TIDE score between the high- and low-risk patients from the TCGA cohort. * $p < 0.05$; ** $p < 0.01$; *** $p < 0.001$; **** $p < 0.0001$

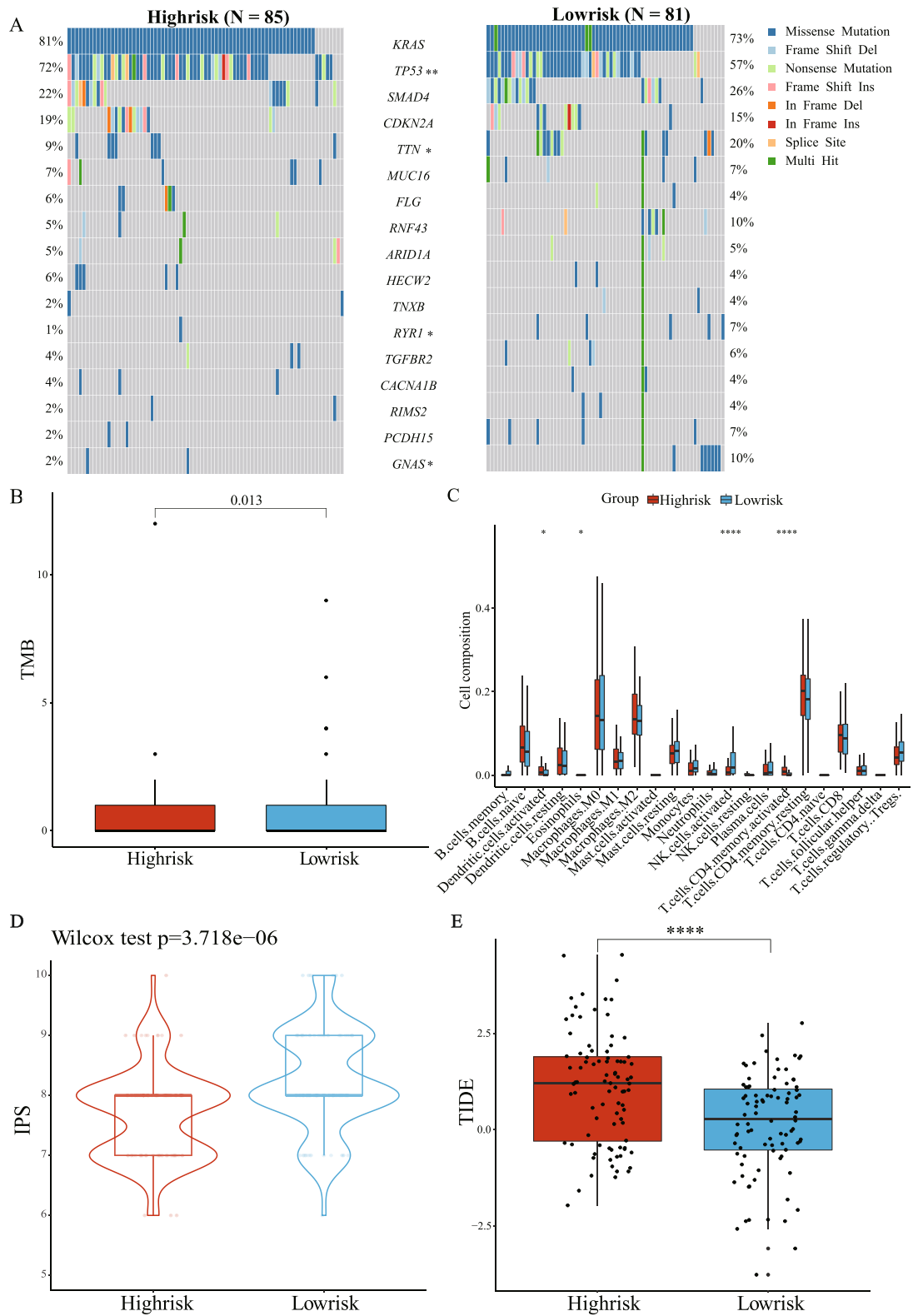


Fig. 5 (See legend on previous page.)

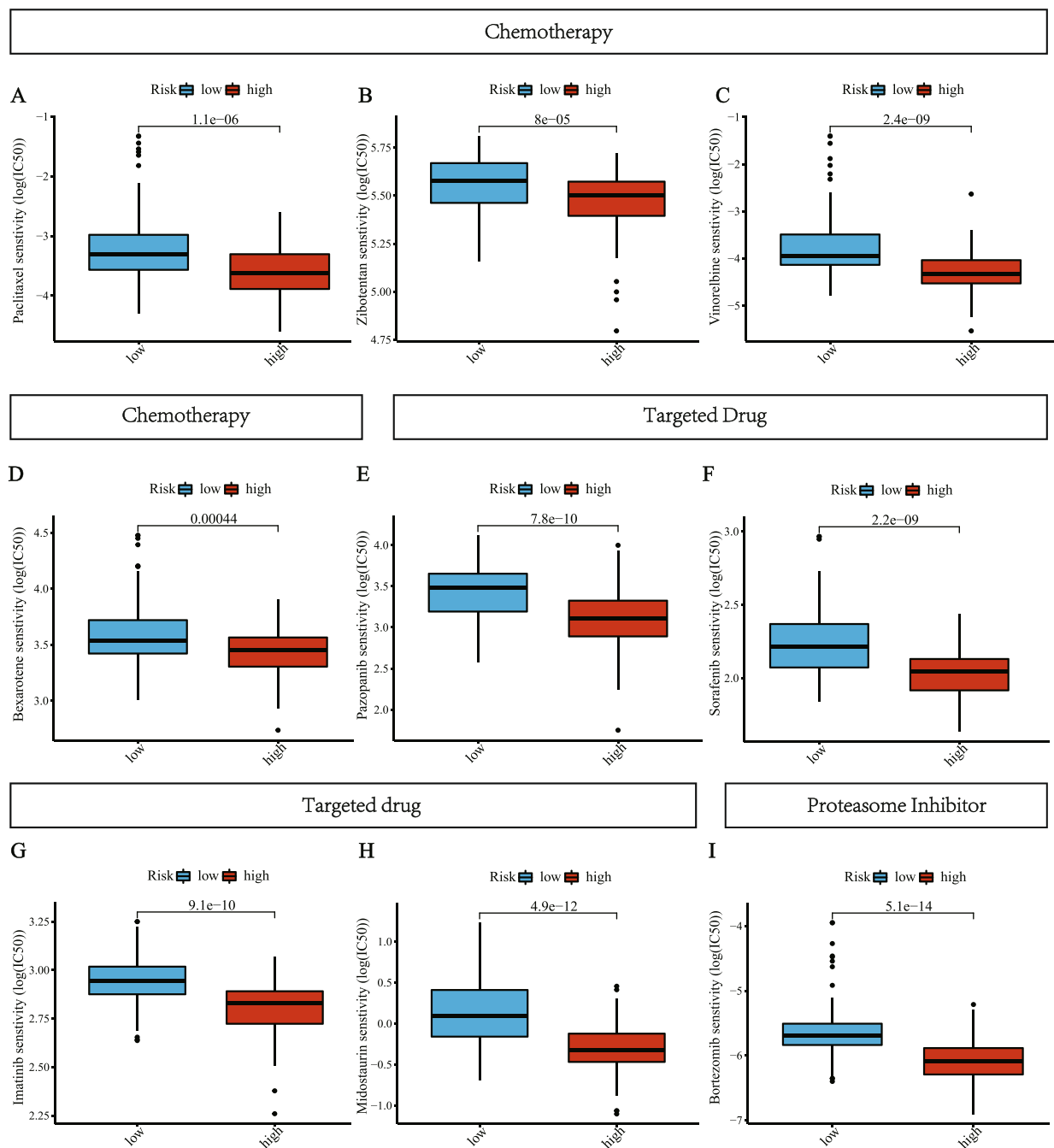


Fig. 6 Association between the risk score and drug sensitivity, including chemotherapeutic and targeted agents, and a proteasome inhibitor. IC50: half-maximal inhibitory concentration

to be an independent predictor of the poor prognosis of PAAD. The higher expression of *TSC22D2* in the pancreatic cancer tissues/cells was also confirmed by the public databases and experiments.

Referring to other signature-based studies, we used the median value of risk score as a cutoff for dividing

patients into the high- and low-risk groups [34, 35]. Our model was verified as a valid and powerful prognostic biomarker for PAAD among three independent cohorts, with worse clinical outcomes in the high-risk patients and better survival in the low-risk patients. Our model's well-established prognostic significance led to the further

investigation of its biological mechanisms. We revealed that DEGs between the risk groups were significantly enriched in several immune-related pathways. Gene mutations were compared between the two risk groups to gain further insight into the immunological nature of the two groups. Consistent with previous studies, missense mutations were the most common mutation type, followed by frameshift deletions and nonsense mutations. The most obvious difference in mutation profiles between the two risk groups was in *TP53* gene mutations, which were significantly more common in the high-risk group than in the low-risk group ($p < 0.01$). Besides, among four major driver genes for PAAD, the high-risk group had a higher frequency of mutation in *KRAS*, and *CDKN2A*. *KRAS* and *CDKN2A* mutation and alterations are early events in the development of pancreatic tumors [29]. *TP53*, the tumor suppressor gene, is mutated in over 70% of pancreatic ductal adenocarcinoma and is frequently linked to invasive and metastatic phenotype [36, 37]. It was proved that patients with *KRAS* or *TP53* mutation showed a worse prognosis than those without mutation ($p = 0.0092$ for *KRAS* and $p = 0.013$ for *TP53*) [38]. Interestingly, *KRAS/TP53* mutations were also demonstrated to be closely associated with immune escape in the mouse PDAC model KPC cells [39]. Therefore, there were relatively higher *TP53* mutations in the high-risk group, which might indicate their poorer prognosis and lesser sensitivity to ICIs.

Subsequently, we analyzed the relationship between the risk groups and known biomarkers for predicting immunotherapy responses, including TMB and MSI. TMB has also been regarded as a potential biomarker for predicting response to ICIs across many tumor types including PAAD [40]. High TMB leads to increased mutation-derived neoantigens that are likely to be recognized by the immune system, making tumors with high TMB more likely to respond to anti-PD-1/PD-L1 therapy [41]. According to our study, high-risk patients demonstrated relatively lower TMB, which might explain why high-risk patients were less likely to respond to ICIs and faced a greater risk of death. Additionally, it has been shown that immunotherapy is effective in rare MSI-high PAAD cases [42]. Thus, we also tested MSI scores in the high- and low-risk groups. However, the difference in MSI between the two risk

groups was not significant. It was probably due to the very low prevalence of MSI in PAAD (1%-2%) [43]. The incidence of MSI was too low to detect a difference between the two risk groups.

The differences in TMEs between the two risk groups might also have important implications for immunotherapy. We revealed different compositions of immune cells between the two risk groups based on the prognostic model. The low-risk group had a higher proportion of activated NK cells and eosinophils than the high-risk group. As infection and tissue damage or inflammatory status occur, eosinophil migration, localization, and activation from the bone marrow were facilitated [44]. Besides, activated NK cells can mediate bone marrow rejection and promote engraftment, and elicit potent anti-tumor effects [45]. Thus, a higher proportion of eosinophils and activated NK cells was related to a better prognosis [44], which was consistent with our results that the low-risk group with more of these cells had a better outcome. In addition, we analyzed the expression of immune checkpoint molecules and found the majority of these molecules were upregulated in the high-risk patients, including PD-1/L1 and CTLA4. Hence, immune response suppression may be existed in the high-risk group of PAAD by "hijacking" the immune checkpoint pathway to achieve immune escape [46].

Both TIDE and IPS have been proven to be superior predictors of the treatment response to anti-CTLA-4 and anti-PD-1 antibodies [25, 47]. The IPS was developed by machine learning using the TCGA data to analyze tumor immunogenicity and tumor escape mechanisms. TIDE is a novel computational method to represent two mechanisms of tumor immune escape: the induction of T cell dysfunction in cytotoxic T lymphocytes (CTL)-high tumors and T cell exclusion in CTL-low tumors [47]. In our study, high-risk patients had higher TIDE and lower IPS scores than low-risk patients. It indicated that high-risk patients had higher levels of immune escape and might be less sensitive to ICI therapies. In addition, we also analyzed drug sensitivity between the high- and low-risk groups. The analyses of nine drugs revealed that patients in the high-risk group may receive benefits more from some chemotherapeutic agents and molecular-targeted drugs. Most of these drugs have been proven

(See figure on next page.)

Fig. 7 The prognostic value and expression of *TSC22D2*. **A** Kaplan–Meier curve for OS between the high- and low-*TSC22D2* expression group in the ICGC cohort. **B** CPTAC website showed the differences in *TSC22D2* expression between cancer tissues and normal tissues at the protein level. **C** Results from GEPIA indicated the relative mRNA expression of *TSC22D2* in PAAD samples and normal samples. **D** Bar chart shows quantification of *TSC22D2* protein levels compared to *GAPDH* control in three independent experiments. One representative blot is shown. Error bars show standard deviation. **E** Assessment of relative fold change in *TSC22D2* mRNA expression (HPNE set as 1) by RT-qPCR, normalized to *GAPDH*. Error bars show standard deviation* $p < 0.05$; ** $p < 0.01$; *** $P < 0.001$; **** $P < 0.0001$. **F** Hematoxylin and eosin (H&E) staining and IHC staining of *TSC22D2* was performed in pancreatic cancer tissues and normal pancreatic tissues. Scale bars: low magnification, 200 μm ; high magnification, 100 μm

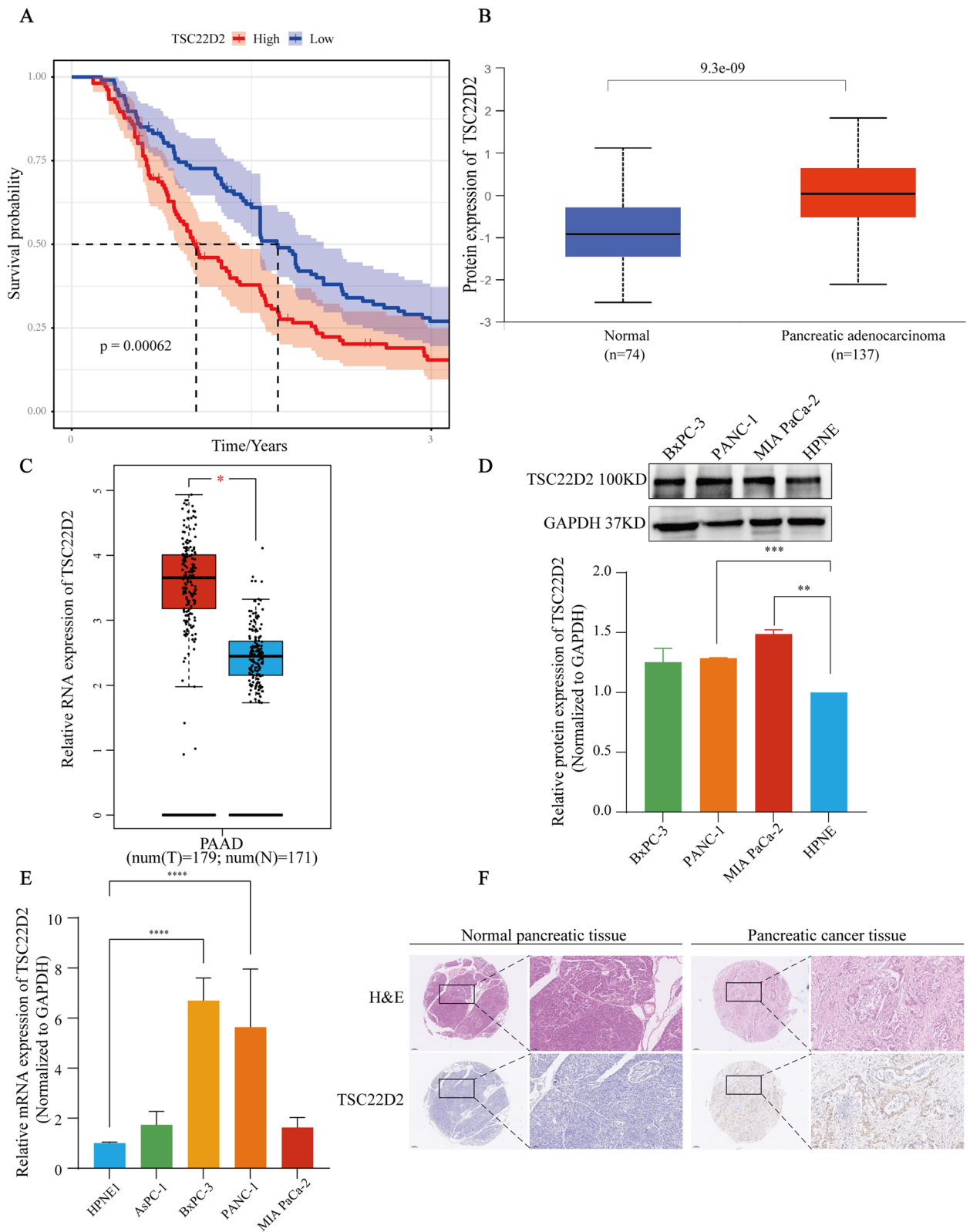


Fig. 7 (See legend on previous page.)

to be effective in treating PAAD patients during clinical trials. For example, nab-paclitaxel plus gemcitabine is a first-line treatment for advanced pancreatic cancer [48]. Sorafenib, an inhibitor of B-raf, VEGFR2, and PDGFR- β , has great activity against pancreatic cancer in a phase I trial [49]. Hence, our prognostic model may be used for optimizing individualized treatments for PAAD patients.

The prognostic model consisted of three cuproptosis-related genes (*PRKDC*, *C6orf136*, *TSC22D2*). Previous research identified that *TSC22D2* was a novel cancer-associated gene in a rare multi-cancer family [50]. In our study, high *TSC22D2* expression was found to act as an independent predictor for the poor prognosis of PAAD. High expression of *TSC22D2* was also related to a significantly higher AJCC tumor stage. However, in colorectal cancer, *TSC22D2* was considered as a tumor suppressor gene, and overexpressed *TSC22D2* inhibited tumor growth [51]. The expression of *TSC22D2* was reported to be significantly downregulated in colorectal cancer, while we found that the expression of *TSC22D2* was significantly higher in pancreatic cancer tissues/cells compared to the normal tissues/cells using public databases and experiments. Thus, *TSC22D2* plays a controversial role in cancers, especially in PAAD. Considering the pivotal role of *TSC22D2* in the process of cuproptosis, depletion of *TSC22D2* would reduce copper-induced cell death. We believe that *TSC22D2* may be utilized as a drug target for PAAD in the future, but the underlying mechanism still needs more research to explore. Additionally, *PRKDC* encodes DNA-dependent protein kinase catalytic subunit (DNA-PKcs), which is crucial for DNA double-strand break repair and V(D)J recombination [52]. Missense mutation of *PRKDC* results in deficient DNA-PKcs, which is associated with the inflammatory disease with organ-specific autoimmunity [53], as well as the loss of mature T and B cells and jak3 in T and putative Natural Killer cells [54]. *C6orf136* is a conserved gene, which is hypermethylated responding to oncogene *FOXMI* expression in head neck squamous cell carcinoma tissue cells [55]. Moreover, *C6orf136* was reported to be a core gene in a signature, which was identified as a novel biomarker for bladder cancer [56]. In the calculation formula of the risk score, the coefficients of *PRKDC* and *TSC22D2* were positive numbers, indicating a positive relationship between the risk score and *PRKDC* and *TSC22D2*. While *C6orf136* was negatively correlated with the risk score. In conclusion, the above studies supported that our prognostic model was a potential measurable prognostic biomarker for PAAD patients.

Although the prognostic model in PAAD is promising, some limitations should be mentioned. First, as

a result of the limited sample size, selection bias may exist. Second, since the number of known cuproptosis-related genes is limited, the model exhibits only moderate efficacy. Third, as the data were mainly obtained from public databases, the actual predictive value of the model needs to be validated with laboratory/real clinical data from large prospective studies prior to clinical application. Finally, the precise roles and molecular mechanisms of cuproptosis-related genes including *TSC22D2* in PAAD have not yet been addressed through biological experiments.

In conclusion, we propose a novel model based on cuproptosis-related genes, which has great potential in predicting prognosis and therapy responses. The precise roles and underlying mechanisms of cuproptosis in PAAD need further explored.

Abbreviations

PAAD	Pancreatic adenocarcinoma
ICGC	International Cancer Genome Consortium
GEO	Gene Expression Omnibus
TCGA	The Cancer Genome Atlas
RT-qPCR	Real-time quantitative PCR
WB	Western blot
OS	Overall survival
HR	Hazards ratios
AJCC	American Joint Committee on Cancer
TCA	Tricarboxylic acid
LDH	Low lactate dehydrogenase
AUC	Area under the curve
KM	Kaplan–Meier
DEG	Differentially expressed gene
FDR	False discovery rate
GO	Gene ontology
TMB	Total mutation burden
MSI	Microsatellite instability
IPS	Immunophenoscore
CTLA-4	Cytotoxic T lymphocyte antigen-4
PD-1	Programmed cell death protein 1
TCIA	The Cancer Immunome Atlas
TIDE	Tumor Immune Dysfunction and Exclusion
ICI	Immune checkpoint inhibitors
GDSC	Genomics of Drug Sensitivity in Cancer
IC50	Half-maximal inhibitory concentration
CPTAC	Clinical Proteomic Tumor Analysis Consortium
FBS	Fetal bovine serum
hTERT-HPNE	Human pancreatic ductal epithelium
CCL	Cancer Cell Line Encyclopedia
CTL	Cytotoxic T lymphocytes
DNA-PKcs	DNA-dependent protein kinase catalytic subunit

Supplementary Information

The online version contains supplementary material available at <https://doi.org/10.1186/s12885-023-10678-9>.

Additional file 1. Supplementary File S1. Cuproptosis-related genes selected by genome-wide CRISPR-Cas9 loss-of-function screens after treatment with elesclomol-copper in OVI5E cells. **Supplementary Table 1.** Differences in clinicopathological characteristics between ICGC training set and ICGC validation set. **Supplementary Figure 1.** The hazard ratio of three genes was calculated by multivariate Cox regression analysis in the prognostic model. **Supplementary Figure 2.** Evaluation of prognostic

model in the GEO testing set. (A) The risk score, survival time, survival status, and 3-gene expression trend in the testing set (GSE85916, 80 samples). (B) ROC curves for the sensitivity and specificity of one-, two-, and three-year OS according to the risk score in the GEO-testing set. (C) Kaplan–Meier curve for OS between the high- and low-risk groups in the GEO-testing set. **Supplementary Figure 3.** Comparison of the molecular characteristics and immunelandscape between the risk groups. (A) Correlation between the risk score and TMB. The Spearman correlation coefficients (R) and corresponding p values are shown. (B) The relationship between the risk score and MSI in TCGA-PAAD cohort. (C) The expression levels of representative immune checkpoint genes in the high- and low-risk PAAD patients from the TCGA cohort. * $p < 0.05$; ** $p < 0.01$; *** $p < 0.001$; **** $p < 0.0001$. **Supplementary Figure 4.** The prognostic value and expression of TSC22D2. (A) Kaplan–Meier curve for OS between the high- and low-TSC22D2 expression groups in the TCGA cohort. (B) The expression of TSC22D2 in pancreatic cancer cells was analyzed in the Cancer Cell Line Encyclopedia database. **Supplementary Figure S1.** (A–B) Original western blot images of TSC22D2 and GAPDH.

Acknowledgements

None.

Authors' contributions

Conception and design: QL. Collection and assembly of data, data analysis, and visualization: QL, HW. Supervision: HW, ZL. Collection and analyses of clinical samples: RL, ZL. The final manuscript was read and approved by all authors. All authors contributed to the article and approved the submitted version.

Funding

This research was supported by CAMS Innovation Fund for Medical Sciences (CIFMS) (No.2021-I2M-1-002), National High Level Hospital Clinical Research Funding (No.2022-PUMCH-B-061), and National Natural Science Foundation of China (No.82072747 and No.82072749).

Availability of data and materials

The datasets generated in this study can be found in The Cancer Genome Atlas (pancreatic adenocarcinoma cohort), International Cancer Genome Consortium (pancreatic adenocarcinoma cohort), and the Gene Expression Omnibus (GEO) (<https://www.ncbi.nlm.nih.gov/geo/>) under the accession numbers GSE85916.

Declarations

Ethics approval and consent to participate

Not applicable. All data in this study are publicly available.

Consent for publication

Not applicable.

Competing interests

The authors declare no competing interests.

Author details

¹Molecular Pathology Research Center, Department of Pathology, Peking Union Medical College Hospital, Chinese Academy of Medical Science & Peking Union Medical College, Beijing, China.

Received: 4 September 2022 Accepted: 24 February 2023

Published online: 10 March 2023

References

- Yu S, Zhang C, Xie KP. Therapeutic resistance of pancreatic cancer: roadmap to its reversal. *Biochim Biophys Acta Rev Cancer*. 2021;1875(1):188461.
- Grossberg AJ, et al. Multidisciplinary standards of care and recent progress in pancreatic ductal adenocarcinoma. *CA Cancer J Clin*. 2020;70(5):375–403.
- Balachandran VP, Beatty GL, Dougan SK. Broadening the impact of immunotherapy to pancreatic cancer: challenges and opportunities. *Gastroenterol*. 2019;156(7):2056–72.
- Shi S, et al. Proposed modification of the 8th edition of the AJCC staging system for pancreatic ductal adenocarcinoma. *Ann Surg*. 2019;269(5):944–50.
- Wang Z, et al. Pancreatic cancer: understanding and overcoming chemoresistance. *Nat Rev Gastroenterol Hepatol*. 2011;8(1):27–33.
- Siegel RL, et al. Cancer statistics 2022. *CA Cancer J Clin*. 2022;72(1):7–33.
- Jiang H, et al. Targeting focal adhesion kinase renders pancreatic cancers responsive to checkpoint immunotherapy. *Nat Med*. 2016;22(8):851–60.
- Michniewicz F, et al. Copper: an intracellular Achilles' heel allowing the targeting of epigenetics, kinase pathways, and cell metabolism in cancer therapeutics. *ChemMedChem*. 2021;16(15):2315–29.
- Oliveri V. Selective targeting of cancer cells by copper ionophores: an overview. *Front Mol Biosci*. 2022;9: 841814.
- Tisato F, et al. Copper in diseases and treatments, and copper-based anticancer strategies. *Med Res Rev*. 2010;30(4):708–49.
- Ishida S, et al. Bioavailable copper modulates oxidative phosphorylation and growth of tumors. *Proc Natl Acad Sci U S A*. 2013;110(48):19507–12.
- Tsvetkov P, et al. Copper induces cell death by targeting lipoylated TCA cycle proteins. *Science*. 2022;375(6586):1254–61.
- O'Day SJ, et al. Final results of phase III SYMMETRY study: randomized, double-blind trial of elesclomol plus paclitaxel versus paclitaxel alone as treatment for chemotherapy-naïve patients with advanced melanoma. *J Clin Oncol*. 2013;31(9):1211–8.
- Zhang G, Sun J, Zhang X. A novel Cuproptosis-related LncRNA signature to predict prognosis in hepatocellular carcinoma. *Sci Rep*. 2022;12(1):11325.
- Lv H, et al. Comprehensive analysis of cuproptosis-related genes in immune infiltration and prognosis in Melanoma. *Front Pharmacol*. 2022;13: 930041.
- Bian Z, Fan R, Xie L. A novel cuproptosis-related prognostic gene signature and validation of differential expression in clear cell renal cell carcinoma. *Genes (Basel)*. 2022;13(5):851.
- Goldman MJ, et al. Visualizing and interpreting cancer genomics data via the Xena platform. *Nat Biotechnol*. 2020;38(6):675–8.
- Troppmann C, et al. Vascular graft thrombosis after pancreatic transplantation: univariate and multivariate operative and nonoperative risk factor analysis. *J Am Coll Surg*. 1996;182(4):285–316.
- Rich JT, et al. A practical guide to understanding Kaplan–Meier curves. *Otolaryngol Head Neck Surg*. 2010;143(3):331–6.
- Kim Y, et al. Nomograms to predict recurrence-free and overall survival after curative resection of adrenocortical carcinoma. *JAMA Surg*. 2016;151(4):365–73.
- Wu T, et al. clusterProfiler 4.0: A universal enrichment tool for interpreting omics data. *Innovation (Camb)*. 2021;2(3):100141
- Lawrence MS, et al. Mutational heterogeneity in cancer and the search for new cancer-associated genes. *Nature*. 2013;499(7457):214–8.
- Mayakonda A, et al. Maftools: efficient and comprehensive analysis of somatic variants in cancer. *Genome Res*. 2018;28(11):1747–56.
- Newman AM, et al. Robust enumeration of cell subsets from tissue expression profiles. *Nat Methods*. 2015;12(5):453–7.
- Charoentong P, et al. Pan-cancer immunogenomic analyses reveal genotype-immunophenotype relationships and predictors of response to checkpoint blockade. *Cell Rep*. 2017;18(1):248–62.
- Bailey JM, et al. Sonic hedgehog promotes desmoplasia in pancreatic cancer. *Clin Cancer Res*. 2008;14(19):5995–6004.
- Bednar F, Pasca di Magliano M. Chemotherapy and tumor evolution shape pancreatic cancer recurrence after resection. *Cancer Discov*. 2020;10(6):762–4.
- Paulson AS, et al. Therapeutic advances in pancreatic cancer. *Gastroenterology*. 2013;144(6):1316–26.
- Kamisawa T, et al. Pancreatic cancer. *Lancet*. 2016;388(10039):73–85.
- Reiss KA, Vonderheide RH. Alternatives to perpetual chemotherapy for metastatic pancreatic cancer. *Clin Cancer Res*. 2021;27(13):3540–2.
- Fan JQ, et al. Current advances and outlooks in immunotherapy for pancreatic ductal adenocarcinoma. *Mol Cancer*. 2020;19(1):32.

32. Neoptolemos JP, et al. Therapeutic developments in pancreatic cancer: current and future perspectives. *Nat Rev Gastroenterol Hepatol*. 2018;15(6):333–48.
33. Li R, et al. Identification and validation of immune molecular subtypes in pancreatic ductal adenocarcinoma: implications for prognosis and immunotherapy. *Front Immunol*. 2021;12: 690056.
34. Hou Y, et al. Comprehensive analysis of a cancer-immunity cycle-based signature for predicting prognosis and immunotherapy response in patients with colorectal cancer. *Front Immunol*. 2022;13: 892512.
35. Chen Y, et al. An immune-related gene prognostic index for head and neck squamous cell carcinoma. *Clin Cancer Res*. 2021;27(1):330–41.
36. Morris JPT, et al. α -Ketoglutarate links p53 to cell fate during tumour suppression. *Nature*. 2019;573(7775):595–9.
37. Makohon-Moore A, Iacobuzio-Donahue CA. Pancreatic cancer biology and genetics from an evolutionary perspective. *Nat Rev Cancer*. 2016;16(9):553–65.
38. Kaushik AC, et al. Irinotecan and Vandetanib create synergies for treatment of pancreatic cancer patients with concomitant TP53 and KRAS mutations. *Brief Bioinform*. 2021;22(3):bbaa149.
39. Hashimoto S, et al. ARF6 and AMAP1 are major targets of KRAS and TP53 mutations to promote invasion, PD-L1 dynamics, and immune evasion of pancreatic cancer. *Proc Natl Acad Sci U S A*. 2019;116(35):17450–9.
40. Maleki VS. High and low mutational burden tumors versus immunologically hot and cold tumors and response to immune checkpoint inhibitors. *J Immunother Cancer*. 2018;6(1):157.
41. Rozeman EA, et al. Survival and biomarker analyses from the OpACIN-neo and OpACIN neoadjuvant immunotherapy trials in stage III melanoma. *Nat Med*. 2021;27(2):256–63.
42. De Dosso S, et al. Treatment landscape of metastatic pancreatic cancer. *Cancer Treat Rev*. 2021;96: 102180.
43. Luchini C, et al. Comprehensive characterisation of pancreatic ductal adenocarcinoma with microsatellite instability: histology, molecular pathology and clinical implications. *Gut*. 2021;70(1):148–56.
44. Davis BP, Rothenberg ME. Eosinophils and cancer. *Cancer Immunol Res*. 2014;2(1):1–8.
45. Hallett WH, Murphy WJ. Natural killer cells: biology and clinical use in cancer therapy. *Cell Mol Immunol*. 2004;1(1):12–21.
46. Liu Z, et al. A novel immune classification reveals distinct immune escape mechanism and genomic alterations: implications for immunotherapy in hepatocellular carcinoma. *J Transl Med*. 2021;19(1):5.
47. Jiang P, et al. Signatures of T cell dysfunction and exclusion predict cancer immunotherapy response. *Nat Med*. 2018;24(10):1550–8.
48. Zhang Y, et al. Nab-paclitaxel plus gemcitabine as first-line treatment for advanced pancreatic cancer: a systematic review and meta-analysis. *J Cancer*. 2019;10(18):4420–9.
49. Kindler HL, et al. Gemcitabine plus sorafenib in patients with advanced pancreatic cancer: a phase II trial of the university of Chicago phase II consortium. *Invest New Drugs*. 2012;30(1):382–6.
50. Xiao L, et al. TSC22D2 identified as a candidate susceptibility gene of multi-cancer pedigree using genome-wide linkage analysis and whole-exome sequencing. *Carcinogenesis*. 2019;40(7):819–27.
51. Liang F, et al. TSC22D2 interacts with PKM2 and inhibits cell growth in colorectal cancer. *Int J Oncol*. 2016;49(3):1046–56.
52. Mathieu AL, et al. PRKDC mutations associated with immunodeficiency, granuloma, and autoimmune regulator-dependent autoimmunity. *J Allergy Clin Immunol*. 2015;135(6):1578–1588.e5.
53. Sun X, et al. DNA-PK deficiency potentiates cGAS-mediated antiviral innate immunity. *Nat Commun*. 2020;11(1):6182.
54. Moore JC, et al. Single-cell imaging of normal and malignant cell engraftment into optically clear prkdc-null SCID zebrafish. *J Exp Med*. 2016;213(12):2575–89.
55. Hwang S, et al. Identification of FOXM1-induced epigenetic markers for head and neck squamous cell carcinomas. *Cancer*. 2013;119(24):4249–58.
56. Tao T, et al. Cancer stem cell-specific expression profiles reveal emerging bladder cancer biomarkers and identify circRNA_103809 as an important regulator in bladder cancer. *Aging (Albany NY)*. 2020;12(4):3354–70.

Publisher's Note

Springer Nature remains neutral with regard to jurisdictional claims in published maps and institutional affiliations.

Ready to submit your research? Choose BMC and benefit from:

- fast, convenient online submission
- thorough peer review by experienced researchers in your field
- rapid publication on acceptance
- support for research data, including large and complex data types
- gold Open Access which fosters wider collaboration and increased citations
- maximum visibility for your research: over 100M website views per year

At BMC, research is always in progress.

Learn more biomedcentral.com/submissions

